# Validation of MELCOR 2.2 Condensation Models for i-SMR Passive Safety Systems

Hanbang Yoo[a], Yejung Jo[a], Yeon-Gun Lee[a*]
[a]*Department of Quantum and Nuclear Engineering, Sejong University*
*209, Neungdong-ro, Gwangjin-gu, Seoul, Republic of Korea*
**Corresponding author: yglee@sejong.ac.kr*
***Keywords :** i-SMR, MELCOR, passive safety systems, condensation, condensation model validation

## 1. Introduction

MELCOR is widely used for integral severe-accident analysis of nuclear power plants. The innovative Small Modular Reactor (i-SMR) relies on passive condensation systems for long-term heat removal. Its accident assessment therefore requires reliable predictions of pressure and heat removal. However, MELCOR's built-in condensation models have not been systematically validated across the horizontal, inclined, and vertical geometries used in these systems.

As shown in Fig. 1, the i-SMR passive safety systems include the Passive Auxiliary Feedwater System (PAFS) and Passive Containment Cooling System (PCCS). The PAFS condenses steam inside submerged horizontal or inclined tubes in a closed natural-circulation loop and returns condensate by gravity. The PCCS removes containment heat by condensation on vertical heat-exchanger surfaces. Because their condensation surfaces and boundary conditions differ, relevant separate-effects data are required before system-level application. This study evaluates MELCOR against horizontal, inclined, and vertical-tube experiments under pure-steam and steam with noncondensable gas (NCG) conditions. Integral heat-removal rates and local heat-transfer coefficients are compared using a common predicted-to-measured ratio to quantify bias, trends, and the validation domain for i-SMR safety assessment.

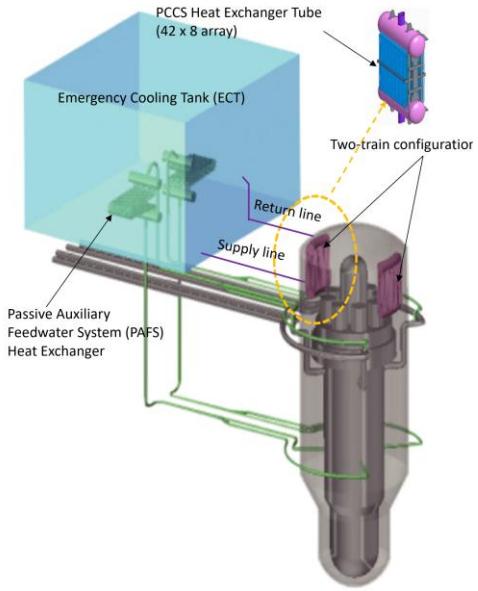



Fig. 1. i-SMR PAFS and PCCS configuration

## 2. MELCOR condensation models

All calculations were performed with MELCOR 2.2.21402. For pure steam, condensation is governed mainly by the liquid film and wall heat transfer. With an NCG, MELCOR applies the stagnant-gas-film formulation described in the MELCOR 2.2 Reference Manual [1], in which vapor diffuses through an NCG-rich boundary layer before condensing at the interface according to Eq. (1):

$$G_c = h_D \rho_v \ln\left(\frac{P_{tot} - P_{surf}}{P_{tot} - P_{stm}}\right) \quad (1)$$

In Eq. (1), $G_c$, $h_D$, and $\rho_v$ are the condensation mass flux, mass-transfer coefficient, and vapor density. $P_{tot}$, $P_{stm}$, and $P_{surf}$ denote the total, bulk-steam, and interfacial saturation pressures. Increasing the NCG fraction reduces the partial-pressure driving force and suppresses condensation.

The mass-transfer coefficient is obtained from the Sherwood number, vapor diffusivity D, and characteristic length $L_c$. The heat- and mass-transfer analogy is expressed by Eq. (2) using the Nusselt, Schmidt, and Prandtl numbers:

$$h_D = \frac{Sh\, D}{L_c}, \quad Sh\, Pr^{0.33} = Nu\, Sc^{0.33} \quad (2)$$

Thus, the gas-side resistance depends on the selected convection correlation and the characteristic geometry assigned to the heat structure.

MELCOR next evaluates the condensate film from the inlet and outlet film flow rates, wetted perimeter w, liquid properties, and the gravity component along the surface according to Eq. (3):

$$Re_f = \frac{2(m_{in} + m_{out})}{w\, \mu_f}, \quad \delta^* = \left(\frac{\mu_f^2}{\rho_f^2 g \sin\theta}\right)^{0.33} \quad (3)$$

In Eq. (3), $m_{in}$ and $m_{out}$ are the boundary film flow rates, while $\rho_f$, $\mu_f$, and $\theta$ are the film density, viscosity, and surface angle. The representative film thickness follows Eqs. (4) and (5), depending on flow regime:

$$\delta_f = 0.909\, \delta^* Re_f^{0.33} \left(Re_f < 1000\right) \quad (4)$$

$$\delta_f = 0.115\, \delta^* Re_f^{0.6} \left(Re_f > 3000\right) \quad (5)$$

Equations (4) and (5) use $Re_f < 1000$ and $Re_f > 3000$ as laminar and turbulent limits, with interpolation in between. One film thickness per heat structure cannot resolve horizontal-tube upper-lower asymmetry.

The film heat-transfer coefficient follows Eqs. (6) and (7), where $k_f$ is the film conductivity:

$$h_f = \frac{k_f}{\delta_f}, Re_f < 1000; \quad h_f = \left(\frac{k_f}{\delta^*}\right) Nu_{f,t}, Re_f > 3000 \quad (6)$$

$$Nu_{f,t}^2 = Re_f^{-\frac{11}{25}} + 5.82 \times 10^{-6} Re_f^{\frac{4}{5}} Pr_f^{0.33} \quad (7)$$

Equations (1)-(7), summarized in Fig. 2, connect vapor diffusion, film transport, and wall heat flux. This averaged formulation is efficient for integral calculations but may limit local predictions when film redistribution or tube orientation produces strong spatial variation.

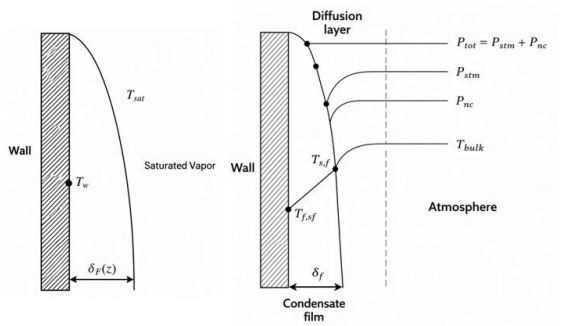



Fig. 2. Condensation models for pure steam (left) and NCG (right)

## 3. Validation results for condensation experiments

Table I summarizes the condensation surfaces and conditions relevant to the PAFS and PCCS. Experiment-specific pressure, inlet steam or gas inventory, and coolant or wall-temperature boundary conditions were imposed, and quasi-steady MELCOR predictions were compared with measured values. The predicted-to-measured ratio R is defined as $Q_{pred}/Q_{meas}$ for integral heat removal and $h_{pred}/h_{meas}$ for local heat transfer. R = 1 indicates exact agreement. R ranges and fractions within ±30% or ±50% are reported where the source data permit. Because no single experiment reproduces the complete i-SMR geometry and accident envelope, the analyzed conditions define a model-level validation domain and identify condition-dependent bias rather than establishing full system validation.

Table I: Condensation-test conditions

| Test | Orientation | Surface | NCG mass fraction | Pressure [MPa] |
|---|---|---|---|---|
| PURDUE | Horizontal | Inner | 0.20 | 0.10-0.40 |
| JAEA | Horizontal | Inner | 0.010 | 0.70 |
| NOKO | Inclined | Inner | 0 | 1.0-7.1 |
| PASCAL | Inclined | Inner | 0 | 0.15-6.7 |
| SNU | Vertical | Outer | 0.05-0.70 | 0.40-2.00 |
| HEU | Vertical | Outer | 0.11-0.71 | 0.20-1.60 |
| KAIST | Vertical | Inner | 0 | 0.35-7.50 |
| ZZU | Vertical | Outer | 0.02-0.82 | 0.21-4.12 |

### *3.1. Horizontal and inclined-tube condensation experiments*

**3.1.1. Experiments and modeling.** The PURDUE experiment [2] and the Japan Atomic Energy Agency (JAEA) experiment [3] provide horizontal-tube steam-NCG condensation data. PURDUE uses a 3.0-m tube, whereas JAEA divides a longer test section into secondary cooling zones. NOKO [4] investigates pure-steam condensation in a 9.8-m tube with 1.6° and 3.2° sections. PASCAL [5] uses an approximately 3° inclined U-tube under pure-steam conditions. Together, these tests cover the main in-tube condensation geometries relevant to the PAFS.

Each test tube was divided into axial control volumes connected by flow paths. Heat structures coupled the primary steam-condensate region to the secondary coolant. In the representative PASCAL model (Fig. 3), the primary side follows the approximately 3° inclined tube, and surrounding pool volumes represent the secondary side. Measured inlet steam, pressure, and coolant conditions were imposed at the boundaries. The JAEA cooling zones and NOKO inclination changes were retained.

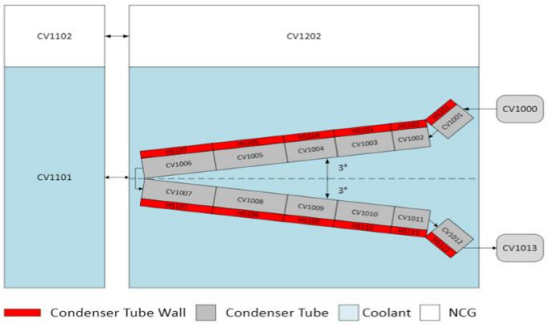



Fig. 3. MELCOR nodalization of PASCAL

**3.1.2. Analysis results.** Fig. 4 compares overall heat removal and local heat-transfer coefficients. Overall heat-removal ratios were R = 0.80-0.91 for PURDUE, 0.56-0.88 for NOKO, and 0.68-0.70 for PASCAL. All PURDUE cases were within ±30%, all NOKO cases were within ±50%, and PASCAL was underpredicted by about 30%. In NOKO, measured heat removal increased with inlet steam flow at each pressure, but MELCOR did not reproduce the monotonic trend. This suggests that the prescribed secondary-side temperature dominated the steam-flow effect.

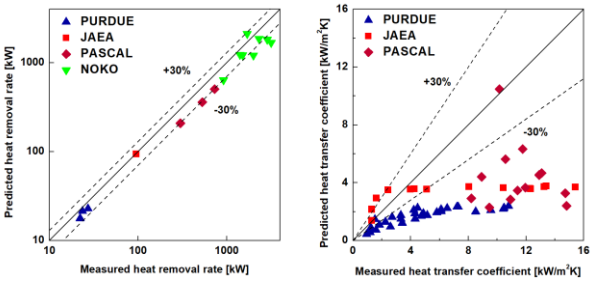



Fig. 4. Horizontal and inclined-tube validation results

Local coefficients were predominantly underpredicted: R = 0.38 for PURDUE, 0.34 for PASCAL, and 0.33 for JAEA, although JAEA was overpredicted at high coefficients. Most PASCAL cases were outside ±50%. This low bias is consistent with MELCOR's single representative film thickness, which cannot resolve circumferential redistribution and upper-lower asymmetry. Under NCG conditions, the gas-side model also does not fully distinguish planar and cylindrical geometries.

Overall heat removal integrates the full condenser response, including secondary-side boundary effects, whereas the local coefficient derives from local heat flux and wall-to-saturation temperature difference. Therefore, closer agreement in overall performance does not demonstrate equivalent local accuracy.

### *3.2. Vertical-tube condensation experiments*

**3.2.1. Experiments and modeling.** Seoul National University (SNU) [6], Harbin Engineering University (HEU) [7], and Zhengzhou University (ZZU) [8] investigate external steam-NCG condensation on a cooled vertical tube relevant to the PCCS. Wall-subcooling ranges are 40-80 K for SNU, 40.6-125.8 K for the analyzed HEU subset, and 8.56-10.64 K for ZZU. The Korea Advanced Institute of Science and Technology (KAIST) instead provides pure-steam in-tube condensation data over a broad pressure range [9].

SNU and ZZU form pressurized steam-nitrog41en atmospheres around a central vertical cooling tube and were used for external-condensation validation. In the nodalization shown in Fig. 5, the chamber gas space was divided into six connected control volumes to permit natural circulation. The cooling-tube wall was represented by two heat structures, and a control function set the coolant-side temperature to match the measured wall subcooling. Steam supply and nitrogen inventory maintained the test pressure and NCG mass fraction before the predicted and measured condensation heat-transfer coefficients were compared.

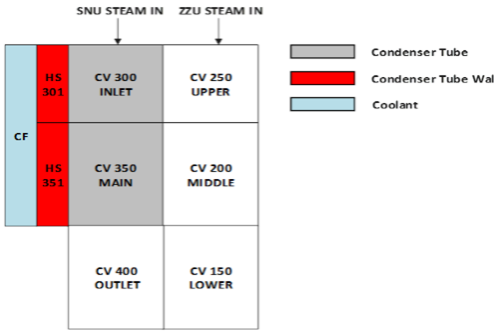



Fig. 5. MELCOR nodalization of SNU and ZZU

The other vertical tests used the same boundary-condition principle with geometry-specific axial control volumes and heat structures. For KAIST, the steam region inside the tube, the tube wall, and the secondary cooling pool were modeled as a coupled thermal system.

**3.2.2. Analysis results.** Fig. 6 compares overall heat-transfer coefficients for external condensation. SNU was predominantly underpredicted (R = 0.56) but mostly within ±50%; MELCOR reproduced the qualitative increase with pressure and decrease with NCG fraction. ZZU gave R = 1.13 and was mostly within ±50%. It tended to be overpredicted at low pressure and NCG fraction, with mixed bias and greater scatter at high values.

For HEU, MELCOR underpredicted 96.3% of cases (R = 0.63), and 85.3% were within ±50%. At NCG mass fraction 0.50, R rose from 0.51 at 0.40 MPa to 0.62 at 1.30 MPa. At 1.30 MPa, it fell from 0.67 at NCG fraction 0.15 to 0.52 at 0.71. Thus, underprediction weakened with pressure and intensified with NCG fraction. Because the datasets also differ in subcooling and facility configuration, no single cause can be isolated.

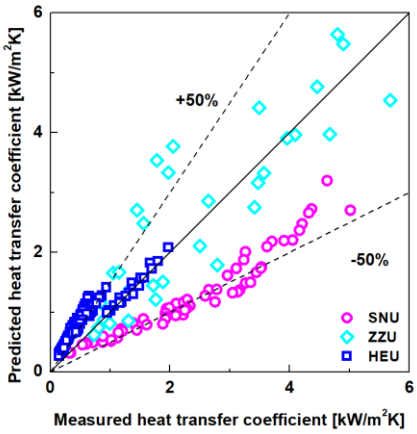



Fig. 6. External condensation results for SNU, ZZU, and HEU

Fig. 7 compares the KAIST pure-steam in-tube results. MELCOR overpredicted the overall heat-transfer coefficient (R = 1.3-2.7), with larger deviations at high pressure. This opposite bias should be distinguished from external steam-NCG condensation. The calculated coefficient couples in-tube condensation, wall conduction, and pool-side heat transfer. Moreover, MELCOR lacks a modified Shah-type in-tube correlation; the overprediction therefore cannot be attributed solely to the condensation model.

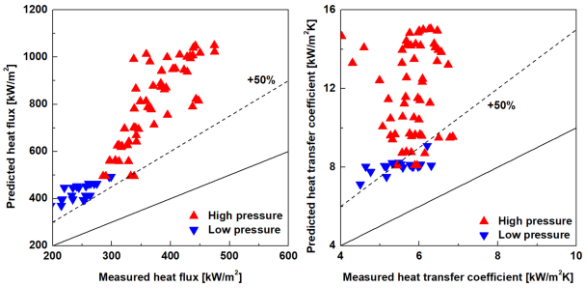



Fig. 7. KAIST heat flux and heat-transfer coefficient results

## 4. Conclusions

Across horizontal and inclined tests, overall heat removal was conservatively predicted with R = 0.80-0.91 for PURDUE, 0.56-0.88 for NOKO, and 0.68-0.70 for PASCAL. Local coefficients showed stronger underprediction (R = 0.38 for PURDUE and 0.34 for PASCAL), so integral agreement did not imply equivalent local accuracy.

For vertical external condensation, R was 0.56 for SNU, 1.13 for ZZU, and 0.63 for HEU. MELCOR captured the qualitative pressure and NCG trends for SNU; HEU underprediction increased with NCG fraction

and decreased with pressure, while ZZU showed condition-dependent scatter. KAIST in-tube coefficients were overpredicted by R = 1.3-2.7, particularly at high pressure. These differing biases indicate configuration- and condition-dependent performance.

These results support limited use of MELCOR for i-SMR system-level trends and integral heat-removal assessments when the applicable test range and bias are documented. However, local condensation heat-transfer coefficients showed large, configuration-dependent discrepancies.

The averaged-film formulation uses one representative film thickness per heat structure and cannot explicitly resolve circumferential film redistribution or the upper-lower film asymmetry of horizontal and inclined tubes. In these tubes, condensate tends to accumulate along the lower surface, leaving a thinner film and lower thermal resistance along the upper surface. Representing these different film thicknesses by a single value may therefore underestimate heat transfer in the thinner-film region. The gas-side model also does not fully distinguish planar and cylindrical geometries. Future work should expand the validation database across pressure, NCG fraction, wall subcooling, and tube orientation, and improve the geometry-dependent film treatment before local coefficients are used quantitatively.

## ACKNOWLEDGEMENTS

This work was supported by the Nuclear Safety Research Program through the Regulatory Research Management Agency for SMRs (RMAS) and the Nuclear Safety and Security Commission (NSSC) of the Republic of Korea (No. 2025-0227-02), and by the Korea Institute of Energy Technology Evaluation and Planning (KETEP) grant funded by the Ministry of Trade, Industry & Energy (MOTIE) (No. 20224B10300050).

## REFERENCES

[1] L. L. Humphries, B. A. Beeny, F. Gelbard, T. Haskin, D. L. Louie, R. C. Schmidt, and N. E. Bixler, MELCOR Computer Code Manuals, Vol. 2: Reference Manual, Version 2.2.18019, SAND2021-0241 O, Sandia National Laboratories, 2021.

[2] T. Wu and K. Vierow, Local Heat Transfer Measurements of Steam/Air Mixtures in Horizontal Condenser Tubes, International Journal of Heat and Mass Transfer, Vol. 49, pp. 2491-2501, 2006.

[3] M. Kondo, H. Nakamura, Y. Kukita, T. Kurita, K. Arai, T. Okazaki, and R. Inoue, Primary-Side Two-Phase Flow and Heat Transfer Characteristics of a Horizontal-Tube PCCS Condenser, Proceedings of ICONE14, Paper ICONE14-89652, Miami, USA, 2006.

[4] A. Schaffrath, E. F. Hicken, H. Jaegers, and H.-M. Prasser, Operation Conditions of the Emergency Condenser of the SWR1000, Nuclear Engineering and Design, Vol. 188, pp. 303-318, 1999.

[5] Y.-J. Cho, S. Kim, B.-U. Bae, Y. Park, K.-H. Kang, and B.-J. Yun, Assessment of Condensation Heat Transfer Model to Evaluate Performance of the Passive Auxiliary Feedwater System, Nuclear Engineering and Technology, Vol. 45, No. 6, pp. 759-766, 2013.

[6] J.-W. Kim, Y.-G. Lee, H.-K. Ahn, and G.-C. Park, Condensation Heat Transfer Characteristic in the Presence of Non-condensable Gas on Natural Convection at High Pressure, Nuclear Engineering and Design, Vol. 239, pp. 688-698, 2009.

[7] H. Bian, Y. Lu, C. Li, T. Liang, and M. Ding, Comprehensive Parameter Analyses on Steam-Air Condensation at Pressures up to 1.6 MPa, Nuclear Engineering and Design, Vol. 385, Article 111536, 2021.

[8] X. Ma, J. Ma, H. Tong, and H. Jia, The Investigation on Heat Transfer Characteristics of Steam Condensation in Presence of Noncondensable Gas under Natural Convection, Science and Technology of Nuclear Installations, Vol. 2021, Article 6689597, 2021.

[9] S. J. Kim, Turbulent Film Condensation of High Pressure Steam in a Vertical Tube of a Passive Secondary Condensation System, Doctoral Dissertation, Korea Advanced Institute of Science and Technology, 2000.